Synthesis and In Situ Atomic Force Microscopy Characterization of Temperature-Responsive Hydrogels Based on Poly(2-(dimethylamino)ethyl methacrylate) Prepared by Atom Transfer Radical Polymerization†

Jinyu Huang,‡ Brian Cusick,‡ Joanna Pietrasik,‡ Li Wang,‡ Tomasz Kowalewski,*,‡ Qiao Lin,*,§ and Krzysztof Matyjaszewski*,‡

Department of Chemistry, Carnegie Mellon University, 4400 Fifth Avenue, Pittsburgh, Pennsylvania 15213, Department of Mechanical Engineering, Carnegie Mellon University, 5000 Forbes Avenue, Pittsburgh, Pennsylvania 15213, and Department of Mechanical Engineering, Columbia University, New York, New York 10027

Received June 12, 2006. In Final Form: August 10, 2006

Well-defined copolymers of 2-(dimethylamino)ethyl methacrylate (DMAEMA) and benzophenone methacrylate (BPMA) with different compositions were synthesized via atom transfer radical polymerization. The molecular weights of these copolymers were $M_n \sim 30\,000$ g/mol, while the BPMA content varied from 2.5 to 10 mol %. The copolymers with a low content of BPMA (2.5 and 5 mol %) exhibited a sharp thermal transition at 33−36 °C in aqueous solution. A hydrogel was immobilized and patterned on a silicon wafer via UV treatment of the spin-coated polymer layer using a photomask technique. The thermoresponsive behavior of the patterned polymer gel was quantitatively investigated by variable temperature in situ contact mode atomic force microscopy, which revealed the presence of two lower critical solution temperature regions. One region was between 25 and 30 °C, corresponding to the topmost layer of the hydrogel film, and the other region, around 40 °C, corresponded to the bulk of the hydrogel. Concurrent lateral force microscopy measurements revealed that, just above the transition temperature, the bulk region exhibited enhanced friction.

Introduction

The surfaces of solid materials can be modified by polymer films to tailor the surface properties such as color, wettability, biocompatibility, adhesion, adsorption, corrosion resistance and friction.[1,2] However, depending on the final application, different thicknesses of the polymer layers are required to efficiently modify the solid substrate. Polymer films can be physisorbed by depositing or spraying a polymeric coating from solution. Alternatively, polymers with reactive end groups can be grafted onto or grafted from surfaces via covalent bonds. If the polymer chains are densely grafted and chains have an extended conformation, polymer brushes are formed.[1,3]

The grafting-from process enables precise control of the grafting density up to ∼1 chain/nm^2 but has limitations in the thickness of the polymer layer up to ∼100 nm due to the limit of polymer chain dimensions. Various well-defined polymers and copolymers have been grafted this way from different kind of substrates. The grafting-onto process has less limitation on the film thickness but results in a much lower grafting density. Several synthetic methods can be used for the preparation of a well-defined attachable copolymer. Atom transfer radical polymerization (ATRP) is compatible with a wide range of functional monomers.[4−10] Thus, ATRP is a powerful technique often used for the synthesis of well-defined (co)polymers with complex architecture and organic/inorganic hybrid materials.[4−9] ATRP has been extensively investigated for the preparation of polymer brushes encompassing a range of compositions and degrees of polymerization that have been used to modify surface properties and prepare nanopattern displays and stimuli-responsive materials.[11−16]

Stimuli-responsive materials have a broad spectrum of potential applications. By changing the composition of the brush, the materials can respond to a variety of external stimuli such as temperature, electric or magnetic field, light, or pH.[17−30] However,

† Part of the Stimuli-Responsive Materials: Polymers, Colloids, and Multicomponent Systems special issue.

* Corresponding author. E-mail: tomek@andrew.cmu.edu (T.K.); ql2134@columbia.edu (Q.L.); km3b@andrew.cmu.edu (K.M.).

‡ Carnegie Mellon University.

§ Columbia University.

(1) Advincula, R.; Brittain, W. J.; Caster, K. C.; Ruhe, J. *Polymer Brushes*; Wiley-VCH Verlag GmbH & Co. KGaA: Weinheim, Germany, 2004.
(2) Zhao, B.; Brittain, W. J. *Prog. Polym. Sci.* **2000**, *25*, 677−710.
(3) Pyun, J.; Kowalewski, T.; Matyjaszewski, K. *Macromol. Rapid Commun.* **2003**, *24*, 1043−1059.
(4) Wang, J.-S.; Matyjaszewski, K. *J. Am. Chem. Soc.* **1995**, *117*, 5614−5615.
(5) Patten, T. E.; Xia, J.; Abernathy, T.; Matyjaszewski, K. *Science* **1996**, *272*, 866−868.
(6) Patten, T. E.; Matyjaszewski, K. *Acc. Chem. Res.* **1999**, *32*, 895−903.
(7) Matyjaszewski, K. *Chem.−Eur. J.* **1999**, *5*, 3095−3102.
(8) Coessens, V.; Pintauer, T.; Matyjaszewski, K. *Prog. Polym. Sci.* **2001**, *26*, 337−377.
(9) Matyjaszewski, K.; Xia, J. *Chem. Rev.* **2001**, *101*, 2921−2990.
(10) Kamigaito, M.; Ando, T.; Sawamoto, M. *Chem. Rev.* **2001**, *101*, 3689−3745.
(11) Husseman, M.; Malmstroem, E. E.; McNamara, M.; Mate, M.; Mecerreyes, D.; Benoit, D. G.; Hedrick, J. L.; Mansky, P.; Huang, E.; Russell, T. P.; Hawker, C. J. *Macromolecules* **1999**, *32*, 1424−1431.
(12) Matyjaszewski, K.; Miller, P. J.; Pyun, J.; Kickelbick, G.; Diamanti, S. *Macromolecules* **1999**, *32*, 6526−6535.
(13) Zhao, B.; Brittain, W. J.; Zhou, W.; Cheng, S. Z. D. *J. Am. Chem. Soc.* **2000**, *122*, 2407−2408.
(14) von Werne, T. A.; Germack, D. S.; Hagberg, E. C.; Sheares, V. V.; Hawker, C. J.; Carter, K. R. *J. Am. Chem. Soc.* **2003**, *125*, 3831−3838.
(15) Pyun, J.; Jia, S.; Kowalewski, T.; Matyjaszewski, K. *Macromol. Chem. Phys.* **2004**, *205*, 411−417.
(16) Matyjaszewski, K.; Miller, P. J.; Shukla, N.; Immaraporn, B.; Gelman, A.; Luokala, B. B.; Siclovan, T. M.; Kickelbick, G.; Vallant, T.; Hoffmann, H.; Pakula, T. *Macromolecules* **1999**, *32*, 8716−8724.
(17) Ionov, L.; Sidorenko, A.; Stamm, M.; Minko, S.; Zdyrko, B.; Klep, V.; Luzinov, I. *Macromolecules* **2004**, *37*, 7421−7423.
(18) Edmondson, S.; Osborne, V. L.; Huck, W. T. S. *Chem. Soc. Rev.* **2004**, *33*, 14−22.

10.1021/la061683k CCC: $37.00
Published on Web 09/28/2006

Scheme 1. (a) Synthetic Pathway for the Preparation of Poly(DMAEMA-*stat*-BPMA) Copolymers via ATRP; (b) Schematic Representation of Hydrogel Patterning Process

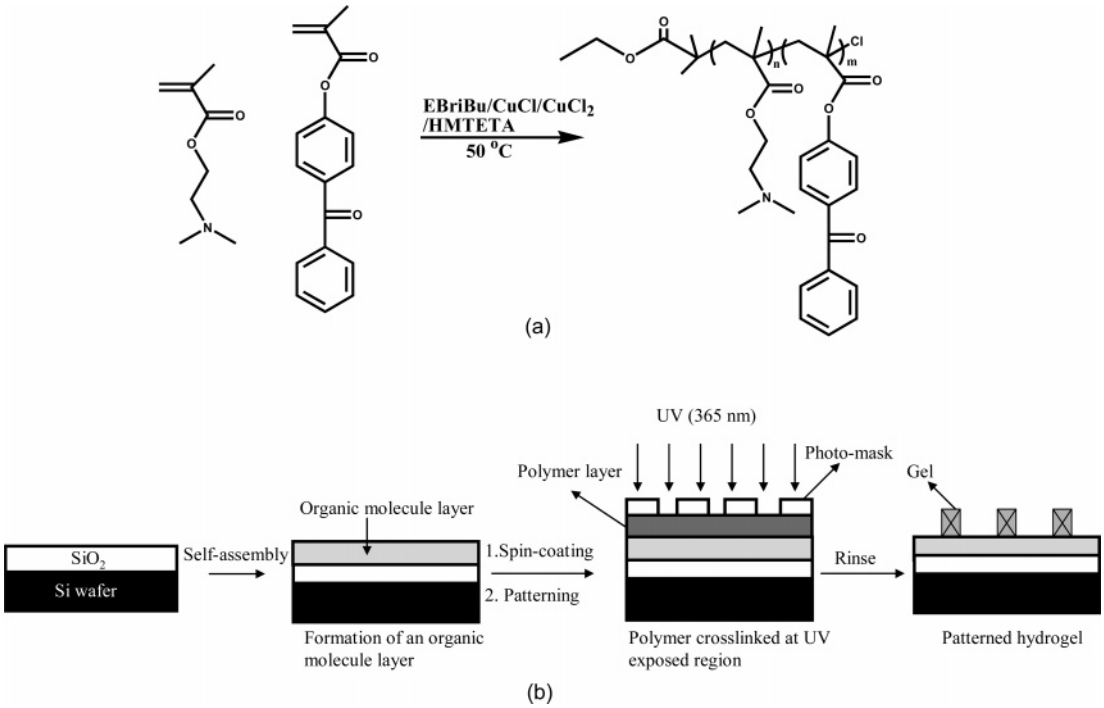

one of the disadvantages of grafting from a surface via ATRP and other controlled radical polymerizations used for polymer brush syntheses lies in the inability of these techniques to prepare thick polymer layers, that is, in the range of micrometers.

Polymer gels have been used to immobilize thick layers of polymers onto solid supports. Most versatile approaches for surface modification with polymer films involve the thermal[31] or photo-cross-linking[32,33] of polymer precursor. Those approaches necessitate the incorporation of some amounts of thermo/photo-cross-linking groups within the polymer precursor.[31,32]

Cross-linked gels prepared from *N*-isopropylacrylamide, vinylmethyl ether, vinyl acetate-*co*-vinyl alcohol, *N*-vinylcaprolactam, and 2-(dimethylamino)ethyl methacrylate (DMAEMA) exhibit discontinuous volume transitions with temperature in aqueous medium.[34−36] When stimuli-responsive gels are attached to the surface, the change in their dimensions as a result of polymer swelling/collapse makes them attractive materials for microfluidic devices, artificial muscles, and tissue engineering.[37−39]

In the work presented herein, we have studied the temperature-responsive behavior of surface-attached poly(2-(dimethylamino)-ethyl methacrylate-*stat*-benzophenone methacrylate) (poly-(DMAEMA-*stat*-BPMA)) gels containing different concentrations of BPMA units.

The gels were composed of well-defined poly(DMAEMA-*stat*-BPMA) copolymers prepared by ATRP. The BPMA units were used as cross-linking moieties.[32,40] This gel was attached onto solid substrates by the deposition of the polymer layer by a standard method for film preparation, followed by subsequent cross-linking.

Patterned hydrogels were obtained by photoinduced cross-linking (using a photomask) of a well-defined polymer layer spin-coated onto the substrate in the presence of coupling agents[41−43] initially attached to an oxidized silicon wafer.[39] The availability of such a pattern can facilitate the characterization of the immobilized gel. The cross-linking and the immobilization of thermoresponsive water-soluble polymers onto the solid support after UV exposure was studied by atomic force microscopy (AFM). The reversible swelling and shrinking behavior of the surface-immobilized gel was monitored quantitatively by following changes in the film thickness by AFM.

Experimental Section

Materials. DMAEMA (Aldrich 99%) was passed through a basic alumina column before use. CuCl was obtained from Aldrich and

(19) Hirokawa, Y.; Tanaka, T.; Katayama, S. *Life Sci. Res. Rep.* **1984**, *31*, 177−188.
(20) Tanaka, T.; Fillmore, D.; Sun, S.-T.; Nishio, I.; Swislow, G.; Shah, A. *Phys. Rev. Lett.* **1980**, *45*, 1636−1639.
(21) Hoffman, A. S. *J. Controlled Release* **1987**, *6*, 297−305.
(22) Tanaka, T.; Nishio, I.; Sun, S. T.; Ueno-Nishio, S. *Science* **1982**, *218*, 467−469.
(23) Osada, Y.; Okuzaki, H.; Hori, H. *Nature* **1992**, *355*, 242−244.
(24) Suzuki, A.; Tanaka, T. *Nature* **1990**, *346*, 345−347.
(25) Matyjaszewski, K. *Prog. Polym. Sci.* **2005**, *30*, 858−875.
(26) Sukhorukov, G.; Fery, A.; Moehwald, H. *Prog. Polym. Sci.* **2005**, *30*, 885−897.
(27) Tanaka, Y.; Gong, J. P.; Osada, Y. *Prog. Polym. Sci.* **2005**, *30*, 1−9.
(28) Gil, E. S.; Hudson, S. M. *Prog. Polym. Sci.* **2004**, *29*, 1173−1222.
(29) Luzinov, I.; Minko, S.; Tsukruk, V. V. *Prog. Polym. Sci.* **2004**, *29*, 635−698.
(30) Lee, H.-i.; Pietrasik, J.; Matyjaszewski, K. *Macromolecules* **2006**, *39*, 3914−3920.
(31) Ryu, D. Y.; Shin, K.; Drockenmuller, E.; Hawker, C. J.; Russell, T. P. *Science* **2005**, *308*, 236−239.
(32) Prucker, O.; Naumann, C. A.; Ruehe, J.; Knoll, W.; Frank, C. W. *J. Am. Chem. Soc.* **1999**, *121*, 8766−8770.
(33) Pahnke, J.; Ruehe, J. *Macromol. Rapid Commun.* **2004**, *25*, 1396−1401.
(34) Panda, A.; Manohar, S. B.; Sabharwal, S.; Bhardwaj, Y. K.; Majali, A. B. *Radiat. Phys. Chem.* **2000**, *58*, 101−110.
(35) Inomata, H.; Goto, S.; Saito, S. *Macromolecules* **1990**, *23*, 4887−4888.
(36) Cheng, S. C.; Feng, W.; Pashikin, I. I.; Yuan, L. H.; Deng, H. C.; Zhou, Y. *Radiat. Phys. Chem.* **2002**, *63*, 517−519.
(37) Buchholz, B. A.; Doherty, E. A. S.; Albarghouthi, M. N.; Bogdan, F. M.; Zahn, J. M.; Barron, A. E. *Anal. Chem.* **2001**, *73*, 157−164.
(38) Kikuchi, A.; Okano, T. *J. Controlled Release* **2005**, *101*, 69−84.
(39) Ito, Y.; Chen, G.; Guan, Y.; Imanishi, Y. *Langmuir* **1997**, *13*, 2756−2759.
(40) Toomey, R.; Freidank, D.; Ruehe, J. *Macromolecules* **2004**, *37*, 882−887.
(41) Revzin, A.; Russell, R. J.; Yadavalli, V. K.; Koh, W. G.; Deister, C.; Hile, D. D.; Mellott, M. B.; Pishko, M. V. *Langmuir* **2001**, *17*, 5440−5447.
(42) Lesho, M. J.; Sheppard, N. F., Jr. *Sens. Actuators, B* **1996**, *37*, 61−66.
(43) Sheppard, N. F., Jr.; Lesho, M. J.; McNally, P.; Francomacaro, A. S. *Sens. Actuators, B* **1995**, *28*, 95−102.

Table 1. Monomer Feed Ratio, Copolymer Composition, and Resulting Properties for the ATRP of DMAEMA and BPMA at $T = 50$ °C

entry	[DMAEMA]/[BPMA] (in the feed monomer)	[DMAEMA]/[BPMA] (in the copolymer[a])	time (h)	DMAEMA conversion[a] (%)	M_n	M_w/M_n
1	400:10	400:10	29	48	31 000	1.22
2	400:20	400:21	29	55	32 800	1.22
3	400:40	400:42	31	46	28 800	1.33

[a] Determined from ^{1}H NMR spectroscopy.

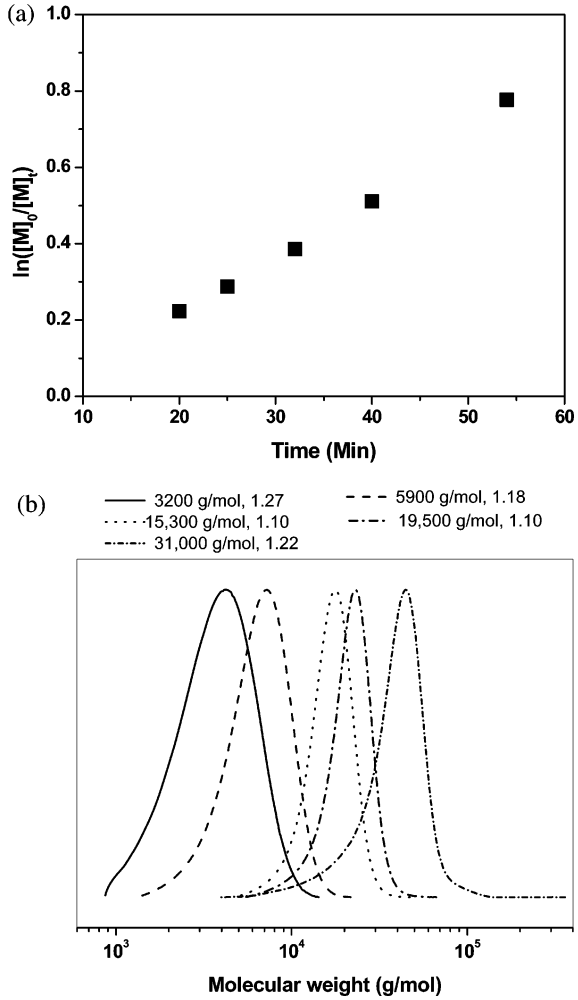

Figure 1. First-order kinetic plot (a) and GPC traces (b) for the copolymerization of DMAEMA and BPMA by ATRP, ([DMAEMA]$_0$/[BPMA]$_0$/[EBriBu]$_0$/[CuCl]$_0$/[$CuCl_2$]$_0$/[HMTETA]$_0$ = 400:10:1:2:0.4:2.4 at 50 °C).

purified by stirring in glacial acetic acid overnight, filtering, and washing with dry ethanol. Trimethoxy(propyl)silane (TMPS) (98%), ethyl 2-bromoisobutyrate (EBriBu) (98%), $CuCl_2$ (98%), 1,1,4,7,-10,10-hexamethyltriethylenetetramine (HMTETA, 97%), methacryloyl chloride (98+%), 4-hydroxybenzophenone (98%), and triethylamine (99.5%) were purchased from Aldrich and used without further purification. All the solvents were obtained from Aldrich unless otherwise stated.

Measurements. Monomer conversion was determined using ^{1}H NMR, which was performed on a Bruker 300 MHz instrument. Molecular weights were analyzed using gel permeation chromatography (GPC) equipped with a Waters WISP 712 Autosampler with dimethylformamide as a solvent, Polymer Standards Service columns (guard, 10^3, 10^5, and 100 Å) in series, and a differential refractometer. Toluene was used as the internal standard, and the molecular weights of the polymers were determined using linear

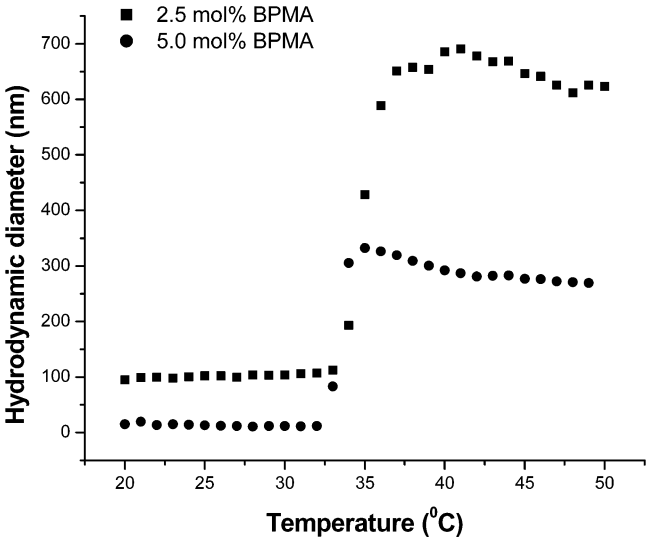

Figure 2. Hydrodynamic diameter of poly(DMAEMA-*stat*-BPMA) copolymers as a function of temperature for aqueous solutions at 1 wt % concentration measured by DLS.

poly(methyl methacrylate) standards. Hydrodynamic diameters (D_H) were determined by dynamic light scattering (DLS) in water with a 1 wt % solution concentration at various temperatures (20−55 °C) with a Malvern HPP5001 high-performance particle sizer. Three measurements were taken for each temperature. Temperature was changed by 1 °C every 6−8 min. AFM studies were conducted using tapping-mode AFM (TMAFM), contact-mode AFM (CMAFM), and lateral force microscopy (LFM). Tapping-mode force microscopy under ambient conditions was carried out with the aid of a Nanoscope III (Veeco Metrology Group, Santa Barbara, CA) equipped with a phase extender module, and a "vertical engage" J-scanner with a sample heating attachment. Tapping-mode imaging in air was carried out with silicon cantilever with a nominal spring constant of 40 N/m (MikroMasch USA, Wilsonville, OR). In situ tapping-mode, contact-mode, and lateral force experiments were carried out with the aid of a fluid cell and a V-shaped silicon nitride cantilever with a nominal spring constant of 0.58 N/m (Veeco Metrology Group, Santa Barbara, CA). This nominal spring constant was used in combination with a contact mode force curve recorded under water on a rigid surface to determine the nominal load, F_n, applied by the tip to the sample. To facilitate the simultaneous acquisition of LFM data, all images were recorded in the fast scan direction perpendicular to the long axis of the cantilever. Scanning at this angle maximizes the torsion of the cantilever and therefore maximizes the lateral force signal. Trace and retrace lateral force images were recorded, and the final lateral force image was obtained by subtracting one from the other. Typical scan sizes ranged from 15 × 15 μm to 60 × 60 μm. The typical scan frequencies were 2 lines per second for TMAFM and 5 lines per second for CMAFM and LFM.

Image Analysis. Analysis of the AFM and LFM images was carried out with the aid of a custom code written in MATLAB 7.0 (The MathWorks Inc., Natick, MA). The images were first flattened line by line using a first-order fit, excluding features above a certain height threshold to avoid baseline artifacts. The flattened images were then thresholded again to isolate the tops of the patches. The tops of the patches, in the thresholded binary images, were then eroded using a circular structuring element with a radius of eight pixels (940 nm), to eliminate patch edge effects. The substrate regions around the patches were identified through a proper combination of successive dilations of the original thresholded image. Height distributions were created from such selected areas of the images. Analysis of the lateral force image used the same masks that isolated the tops of the patches and the substrate for height analysis. Distributions of lateral force were then made for the patch and the substrate regions.

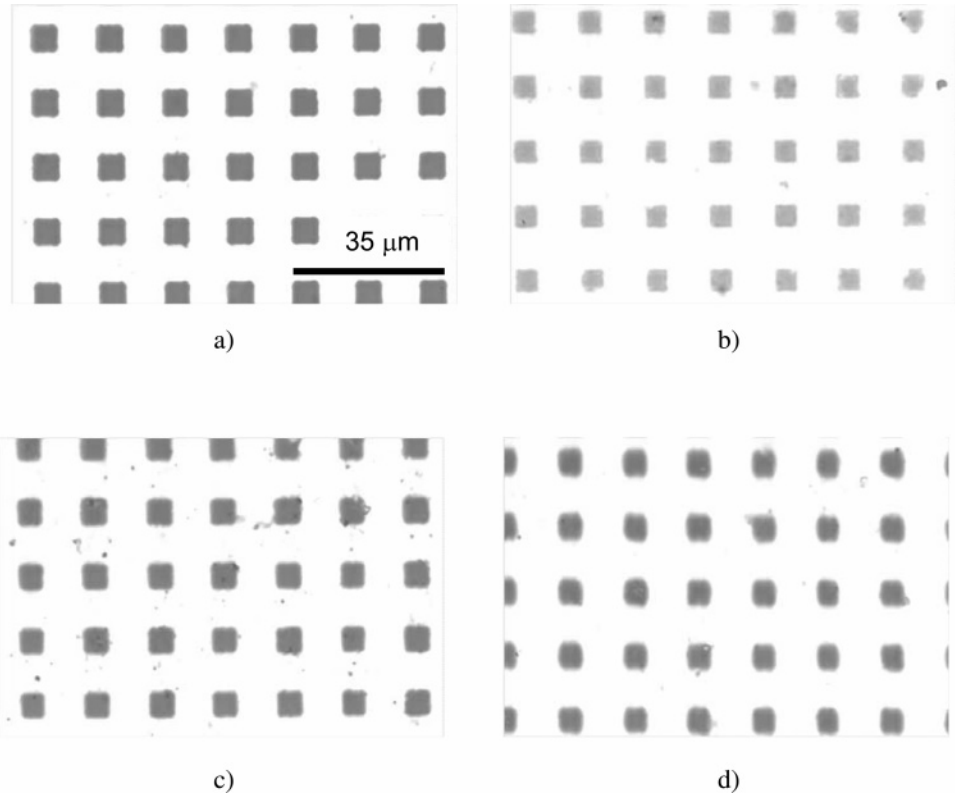

Figure 3. Optical micrographs of a photomask (a) and patterned gels prepared by UV irradiation of poly(DMAEMA-*stat*-BPMA) copolymers (2.5 mol % BPMA) for different exposure times: (b) 2.5 min, (c) 7.5 min, and (d) 10 min.

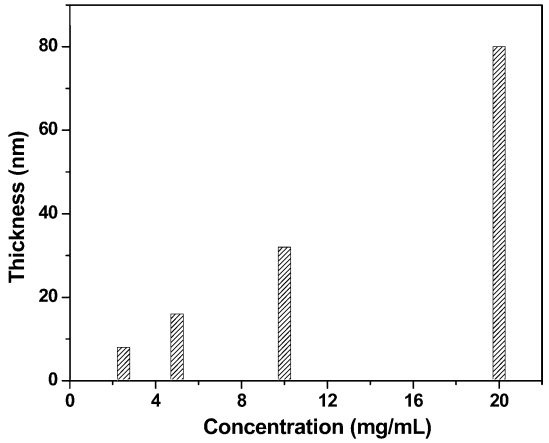

Figure 4. Dependence of copolymer film thickness on the concentration of solutions used in spin-coating.

Synthesis of BPMA. To a solution of 4-hydroxybenzophenone (20.0 g, 101 mmol) and triethylamine (20 mL, 150 mmol) in dichloromethane (DCM) (200 mL), methacryloyl chloride (11.7 mL, 120 mmol) in DCM (50 mL) was added dropwise at 0 °C, and the resulting mixture was stirred at room temperature overnight. The mixture was washed with water (100 mL × 2), a saturated aqueous solution of $NaHCO_3$ (100 mL × 2), and a saturated aqueous solution of NaCl (100 mL). The organic layers were dried over anhydrous $MgSO_4$, filtered, and the solvent was evaporated. The resulting residue was purified by recrystallization from *n*-hexane; yield: 3.2 g (87%); mp: 66−68 °C (69.5−70.5 °C);[44] ^{1}H NMR (300 MHz, $CDCl_3$), δ: 2.11 (s, 3 H, CH_2═C(CH_3)), 5.84 and 6.42 (s, 2 H, CH_2═C(CH_3)), 7.29−7.92 (m, 9 H, phenyl) ppm. IR (KBr): 3049, 2983, 2959, 2926, 1732, 1652, 1596, 1446, 1319, 1280, 1161, 1130, 939, 698 cm^{-1}.

(44) Miyano, M.; Deason, J. R.; Nakao, A.; Stealey, M. A.; Villamil, C. I.; Sohn, D. D.; Mueller, R. A. *J. Med. Chem.* **1988**, *31*, 1052−1061.

Synthesis of poly(DMAEMA-*stat*-BPMA) Copolymers. A typical polymerization procedure was as follows: 4.7 mL (32 mmol) of DMAEMA, 0.19 g (0.71 mmol) of BPMA, 12 μL (0.08 mmol) of EBriBu, 44 μL (0.2 mmol) of HMTETA, and 2 mL of acetone were added to a 10 mL Schlenk flask. After three freeze−pump−thaw cycles, CuCl (16 mg, 0.16 mmol) and $CuCl_2$ (4 mg, 0.032 mmol) were added under N_2. The reaction was carried out at 50 °C. Samples were taken periodically to analyze monomer conversion by ^{1}H NMR and the molecular weight by GPC. The polymerization was stopped by opening the flask to air when the desired molecular weight was reached. The reaction mixture was then diluted with 10 mL of acetone and passed through a small neutral alumina column to remove the catalyst. The final pure product was obtained after precipitation into hexanes.

Photopatterning. The Si wafers were activated by immersing them into a piranha solution (H_2O_2/H_2SO_4 = 3:7 (v/v)) for 1 h, followed by washing with deionized water, tetrahydrofuran, and acetone. A monolayer of organic molecules was introduced onto the Si surface by immersing the wafers in a toluene solution of TMPS (20 mg/mL) with triethylamine as the catalyst. After overnight reaction at 70 °C, the wafers were washed with acetone. The polymer film was deposited on the modified Si surface by spin-coating from a solution in $CHCl_3$ at a velocity of 2000 rpm and an acceleration rate of 2000 rpm. The patterning of the polymer films was performed by exposing them to the UV light (365 nm, 8 mW/cm^2) produced by collimated UV light sources (OAI, San Jose, CA) through a photomask with a feature size of 5 × 5 μm separated by 10 μm.

Results and Discussion

Synthesis of poly(DMAEMA-*stat*-BPMA) Copolymers. Poly(DMAEMA-*stat*-BPMA) copolymers with three different BPMA contents were prepared by ATRP in the presence of CuCl/$CuCl_2$/HMTETA as the catalyst system (Scheme 1, Table 1).

All the copolymerizations proceeded in a controlled manner, leading to copolymers with relatively narrow molecular weight distributions. Figure 1 shows the experimental results for the copolymerization of DMAEMA and BPMA at a molar ratio of

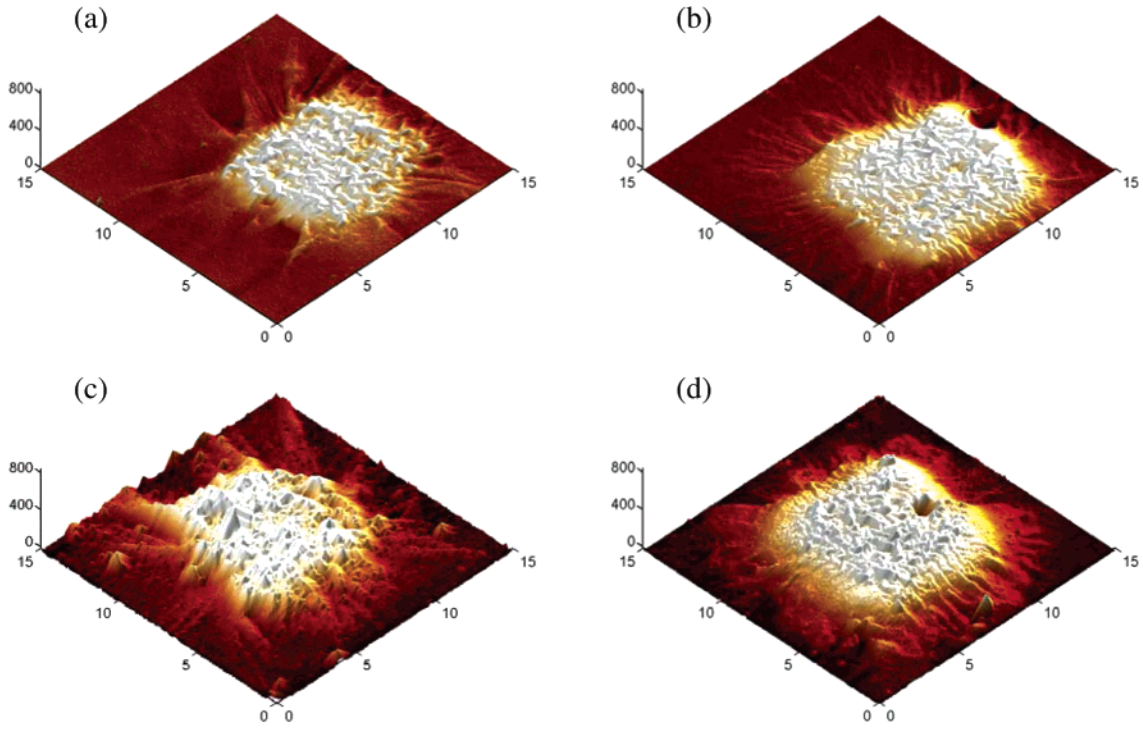

Figure 5. TMAFM height images (15 μm × 15 μm × 850 nm) of individual patches of lithographically patterned and UV-cross-linked thin films of sample **1** (a,c; 2.5% BPMA) and sample **2** (b,d; 5% BPMA) acquired under ambient conditions (a,b) and under water (c,d). Note the significant increase in the height of patches above the surrounding silicon wafer substrate upon hydration (∼50 to ∼250 nm). In both cases, the hydration enhanced the characteristic twisted nodular morphology of the film surfaces.

400:10. Monomer consumption increased linearly with time, following first-order kinetics, and the GPC traces progressively shifted to higher molecular weight during the polymerization.

The fraction of BPMA in the copolymers was controlled by varying the monomer feed ratio because DMAEMA and BPMA have similar reactivity ratios, as shown by the similar composition of the comonomer feed and the resulting copolymers.

The copolymers synthesized within this study and containing 2.5 and 5 mol % of BPMA comonomer exhibited a lower critical solution temperature (LCST) in aqueous solution with the temperature of the phase transition being dependent on the content of hydrophobic BPMA. The 10 mol % sample had an LCST below room temperature and was not further studied. As shown in Figure 2, DLS measurements indicate that the LCST temperatures of the aqueous solution of the copolymers decreased with increasing content of BPMA in the copolymer. Although the thermoresponsive behavior of the free linear polymer in solution is not expected to be identical to that of the gel attached to a surface, information on the phase transition behavior of the free polymer still provides data relevant to the study of the thermoresponsive behavior of the attached gels.

Micropatterning of Hydrogel Films. Scheme 1 shows the approach used to achieve patterned hydrogel films via photopatterning. First, the Si substrate was modified to attach a monolayer of alkyl chains that acted as an adhesion promoter for the deposited patterned gel. This surface modification was achieved by immersing the wafers in a toluene solution of TMPS. The condensation reaction between the trimethoxysilyl groups in TMPS and the surface silanol groups led to the immobilization of the alkyl chains on the surface. A patterned hydrogel film was then prepared by photoirradiation of the spin-coated polymer layer on the modified Si substrate through a photomask with a feature size about 5 × 5 μm separated by 10 μm. The BPMA units in the copolymer act as the cross-linking moiety since irradiation of benzophenone leads to the formation of biradicals that are capable of abstracting the hydrogen from neighboring aliphatic C−H groups, including adjacent polymer chains and the organic layer coated onto the silicon surface.[32] As a result, the exposed part of the film was cross-linked and covalently attached to the substrate. Un-cross-linked polymer in the covered or masked part was completely removed by rinsing with methanol. Thus a negative image of the photomask was obtained. The availability of such a pattern was essential for AFM characterization of the gel thickness change as a function of temperature.

It was found that exposure time is one of the crucial parameters in the preparation of a patterned gel and has to be adjusted with respect to the thickness of the polymer layer. Figure 3 shows the optical micrographs of the patterned gel constructed from the poly(DMAEMA-*stat*-BPMA) copolymer with 2.5 mol % BPMA. When the exposure time was too short (2.5 min) (Figure 3b), a poorly defined pattern was obtained, as some of the patterned microgels lost definition. This is because the short exposure time led to insufficient cross-linking among the polymer chains and an inadequate number of chemical bonds between the gel and the surface. As a result, the gel did not sufficiently adhere to the solid support.

When the exposure time was increased to 7.5 min (Figure 3c), a well-defined pattern of the gel was obtained. The shape of the tethered microgels was identical to that of the photomask. However, when the exposure time was increased to 10 min (Figure 3d), overexposure occurred, as demonstrated by the blurred profile of the gels. Films of different thickness could be obtained by varying the concentration of the polymer in the solution or the spin rate. Figure 4 illustrates that the film thickness increased from 8 to 80 nm when the polymer concentration was increased from 2.5 to 20 mg/mL.

Atomic Force Microscopy. TMAFM images of samples **1** and **2** (Table 1) imaged at room temperature in air and under water are shown in Figure 5. When imaged in air, the mean height of the copolymer film patches was equal to 50 ± 10 nm

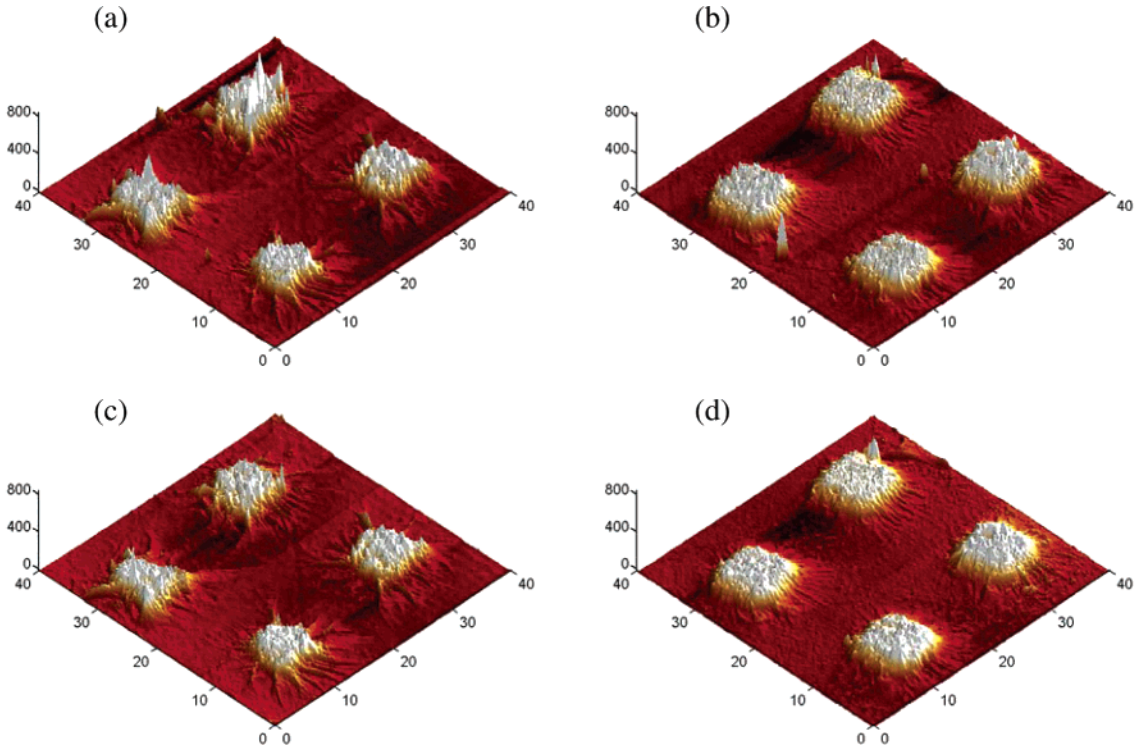

Figure 6. In situ CMAFM height images (40 μm × 40 μm × 850 nm) of several patches of lithographically patterned and UV-cross-linked films of sample **1**, (a,c; 2.5% BPMA) and sample **2** (b,d; 5% BPMA) at 25 °C (a,b) and 60 °C (c,d).

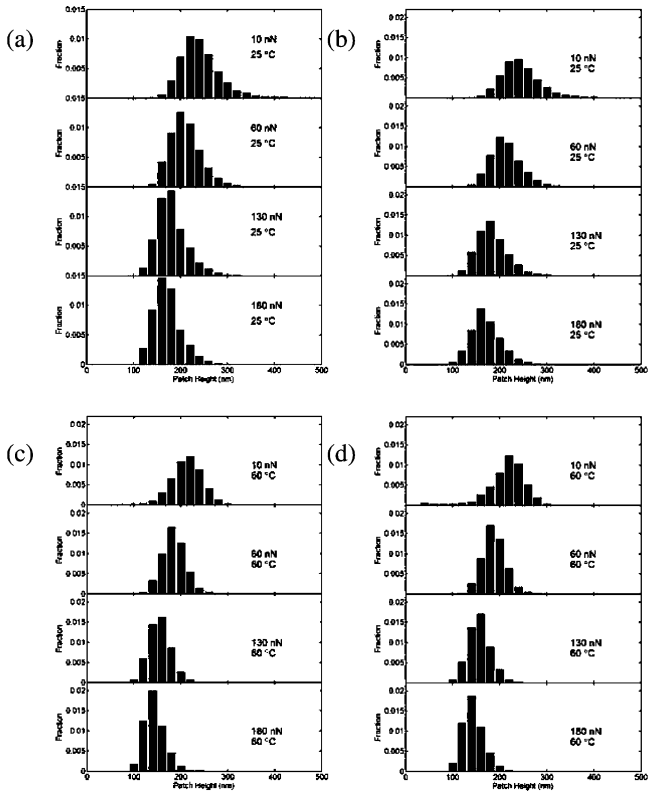

Figure 7. Normalized patch height distributions based on CMAFM images acquired under different nominal loads for sample **1**, (a,c) and sample **2** (b,d) at 25 °C (a,b) and 60 °C (c,d).

for sample **1** (a) and 65 ± 10 nm for sample **2** (b). Both samples exhibited the characteristic twisted nodular morphology and the presence of elongated "tentacle" structures radiating out over the silicon surface far beyond the square-shaped patch outline. The samples were then mounted in the fluid cell and imaged again under water using the tapping mode. Upon immersion in water, the height of the patches exhibited about a 5-fold increase, consistent with the extensive swelling and formation of a hydrogel. The characteristic nodular morphology and "tentacles" persisted in the swollen state.

When the temperature of the fluid cell was increased to 60 °C, that is, far above the LCST of "free" copolymers, the freshly immersed samples exhibited a substantial decrease in height (from ∼250 to ∼150 nm). Upon cooling back to room temperature, the patches reverted back to their original (∼250 nm) heights. However, the initially observed pronounced decrease in height was not observed in subsequent experiments when the fluid cell temperature was varied systematically from room temperature to 60 °C in smaller intervals. Instead, the mean height of the patches fluctuated approximately ±10% around 250 nm, without any clear correlation with temperature. One of the possible reasons for the apparently uncorrelated fluctuations in patch heights with fluid cell temperature can be explained by the high sensitivity of the average tapping force to operating parameters (drive amplitude, frequency, set-point), which, in-turn, are all sensitive to temperature. Difficulties with ensuring consistent tapping-force conditions, which is critical for achieving reliable height measurements in soft materials, prompted us to explore the use of CMAFM, where control of normal force F_n can be achieved much more easily by simply maintaining the proper set-point (cantilever deflection) value Δz, since $F_n = k\Delta z$, where k is the cantilever spring constant. The choice of CMAFM over TMAFM may initially appear counterintuitive since TMAFM is renowned for its suitability for imaging particularly delicate, soft samples. One has to keep in mind, however, that, in operation under fluids, the average tapping force can easily reach quite high values (up to hundreds of nanonewtons),[45−50] and the main advantage of

(45) Humphris, A. D. L.; Round, A. N.; Miles, M. J. *Surf. Sci.* **2001**, *491*, 468−472.
(46) Humphris, A. D. L.; Tamayo, J.; Miles, M. J. *Langmuir* **2000**, *16*, 7891−7894.
(47) Legleiter, J.; DeMattos, R. B.; Holtzman, D. M.; Kowalewski, T. *J. Colloid Interface Sci.* **2004**, *278*, 96−106.

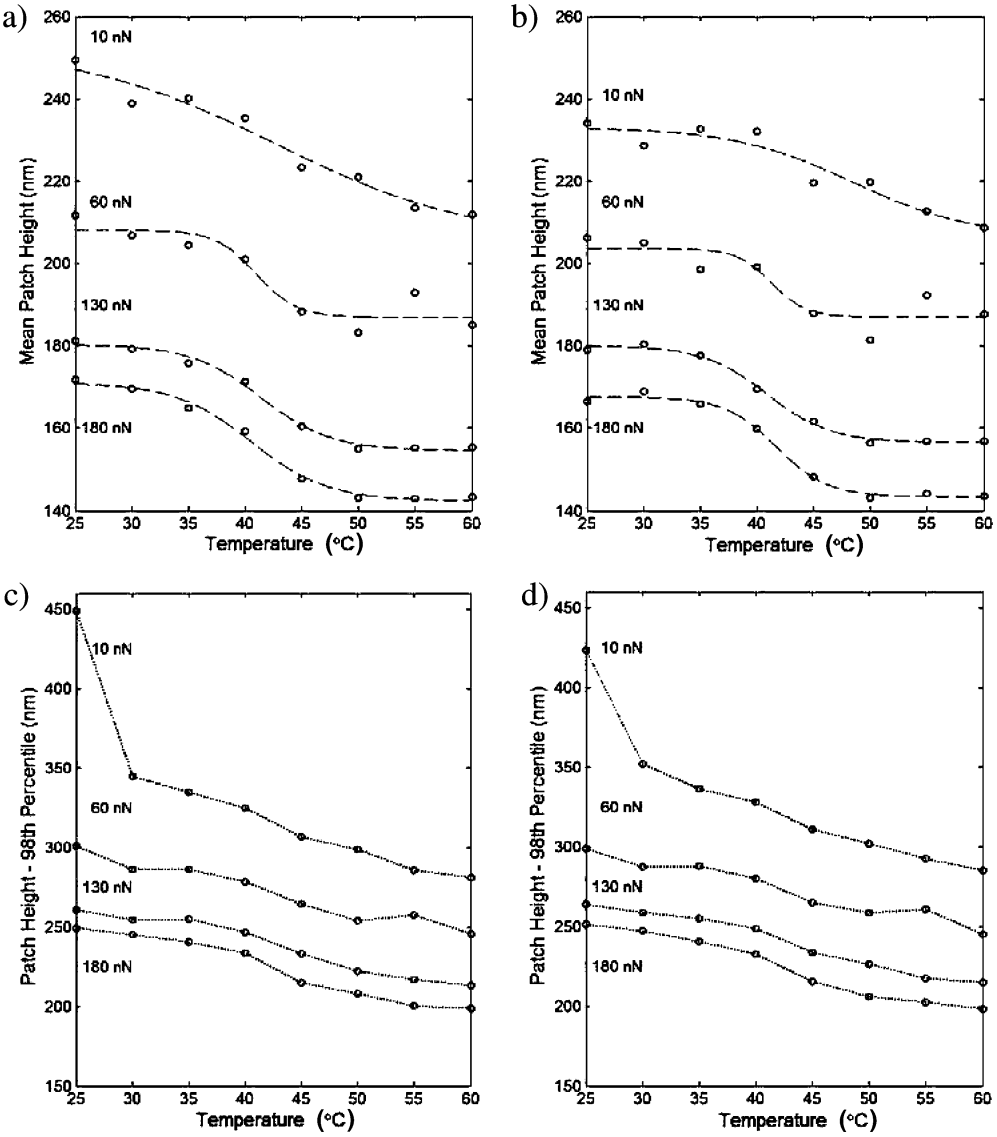

Figure 8. Mean height (top row) and 98th percentile height (bottom row) data as a function of temperature for sample **1** (a,c) and sample **2** (b,d) based on CMAFM images acquired under different loads.

the tapping mode is in eliminating the lateral force, which could irreversibly damage fragile polymer films or "sweep away" individual nano-objects such as biological macromolecules, nanoparticles, and so forth. As will be shown below, with cross-linked films such as those studied here, one does not need to be as concerned about the detrimental effects of lateral force. Moreover, measurements of its spatial variability (LFM) can provide information about local energy dissipation through friction, yielding additional insight into the behavior of the material.[51]

CMAFM images of the same area of samples **1** (a,c) and **2** (b,d) acquired under water at room temperature and at 60 °C with a normal force of $F_n = 130$ nN are shown in Figure 6. The overall morphology of the patches closely resembled the one observed with TMAFM (cf. Figure 5). This time, however, the patch heights at 60 °C showed a clear decrease in comparison with those acquired at room temperature.

More accurate analysis of patch height distributions was carried out using patch height distributions constructed from AFM images by selective masking, as described in the Experimental Section, which assured the elimination of patch edge effects. Examples of such distributions obtained from the images shown in Figure 6 and images acquired in the same area under other normal loads F_n, are shown in Figure 7. The considerable width of these distributions exclusively reflected the local variations of patch heights as a result of their characteristic nodular morphology. As expected for a compressible hydrogel material, the distributions shifted systematically toward lower heights and narrowed down with the increase in normal load.

The distributions changed systematically when the fluid cell temperature was increased in 5 °C intervals from room temperature to 60 °C. Those changes are summarized in Figure 8, which shows the temperature variation of the mean height (a,b) and 98th percentile height (c,d), which was used to characterize the behavior of the top 2% of the tallest features in the distribution.

For both samples, the mean height exhibited a clear drop around 40 °C, that is, at the temperature between the LCST of poly(DMAEMA-*stat*-BPMA) copolymers and the LCST of a DMAEMA homopolymer. At the minimal normal load of 10

(48) Legleiter, J.; Kowalewski, T. *Appl. Phys. Lett.* **2005**, *87*, 163120/163121−163120/163123.
(49) Tamayo, J.; Humphris, A. D. L.; Miles, M. J. *Appl. Phys. Lett.* **2000**, *77*, 582−584.
(50) Tamayo, J.; Humphris, A. D. L.; Owen, R. J.; Miles, M. J. *Biophys. J.* **2001**, *81*, 526−537.
(51) Ruan, J.-A.; Bhushan, B. *J. Tribol.* **1994**, *116*, 378−388.

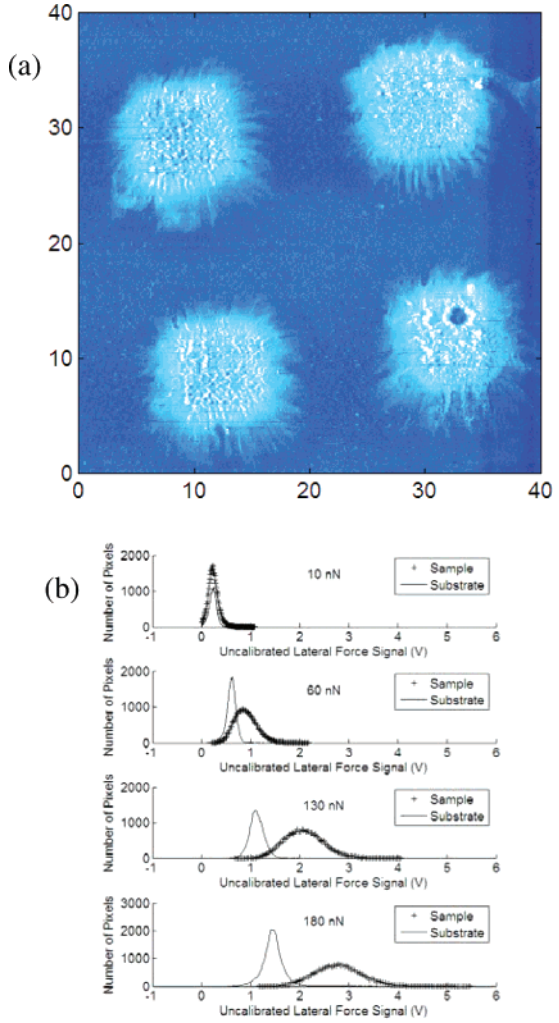

Figure 9. (a) LFM image (40 × 40 μm) of sample **2** acquired under water at 60 °C under a 180 nN load and (b) a distribution of the lateral forces for both the polymer patch and the substrate under different loads.

nN, when the gel was minimally compressed by the tip, the mean height decreased monotonically with temperature, dropping over the whole temperature interval by ∼20−30 nm. At higher loads, when the gel was compressed by the tip by 40−80 nm, the change in height had a character of a rather sharp transition, centered at ∼40 °C. The observed changes of height can be naturally associated with the collapse of DMAEMA copolymer chains above the LCST. As described earlier, the LCST of "free" copolymer chains in solution measured by DLS was in the vicinity of 34 °C (see Figure 2), that is, considerably lower than the reported ∼40 to ∼50 °C LCST of the DMAEMA homopolymer.[52] Such decrease can be easily explained as an effect of the incorporation of BPMA containing hydrophobic benzophenone moieties in the copolymer. The upward shift in the polymer collapse transition in cross-linked poly(DMAEMA-*stat*-BPMA) gels in comparison with that of free copolymer chains in solution suggests that, upon cross-linking, the impact of benzophenone moieties on polymer solubility in water decreased. Let's recall that the transition was much more diffuse at minimized loads, that is, when the AFM probe interacted only with topmost portion of the film. This may suggest some nonuniformity in the degree of cross-linking near the surface, leading to the broad distribution of "free" benzophenone groups capable of adversely impacting

(52) Cho, S. H.; Jhon, M. S.; Yuk, S. H.; Lee, H. B. *J. Polym. Sci., Part B: Polym. Phys.* **1997**, *35*, 595−598.

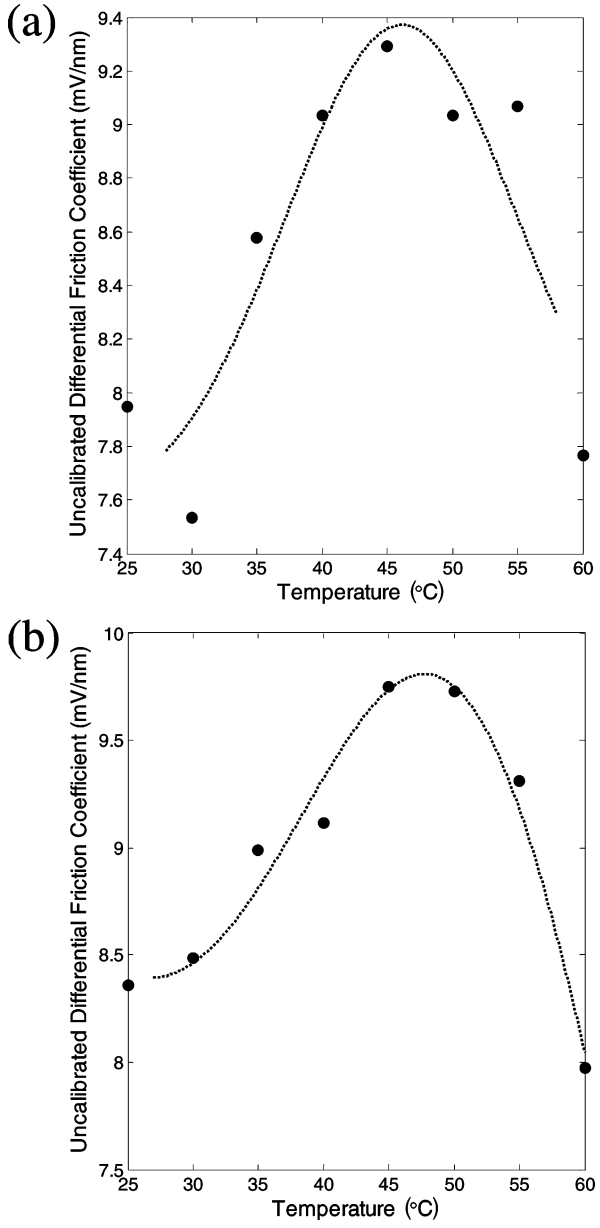

Figure 10. Uncalibrated differential friction coefficient of sample **1** (a) and sample **2** (b) calculated from lateral force images acquired under water at different temperatures (see text).

the polymer solubility. It should be pointed out that the proposed nonuniformity of cross-linking could be also responsible for the peculiar nodular morphology of cross-linked film surfaces.

At this point, we turn the reader's attention to the high end tails of patch height distributions, corresponding to the uppermost tips of nodules observed on the surface. The behavior of these regions is summarized by the 98th percentile plots shown in Figure 8c,d. When imaged at minimal loads at room temperature, these regions extended as high as ∼400 nm above the surface. However, when the temperature of the fluid cell was increased by just 5 °C, their height dropped precipitously by almost 100 nm. At higher temperatures, the height of nodule tips decreased in a fashion similar to the average height of the film. This behavior strongly suggests that the topmost regions of the film were much more weakly cross-linked, behaving more like individual chains in solution.

Results presented so far illustrate the applicability of CMAFM to study the thermal behavior of hydrogel films, particularly

pointing to the advantages of imaging the material at different normal loads, and thus, effectively, to different depths.

Some additional insight into the thermal behavior of poly(DMAEMA-*stat*-BPMA) hydrogels was obtained from the analysis of lateral force images, acquired simultaneously with topographic contact-mode images. An example of an LFM image of a hydrogel sample under water (sample **2**, 60 °C, $F_n = 180$ nN) is shown in Figure 9a. Brighter regions in this image correspond to the areas of higher lateral force signal, S_L. In all cases, the lateral force signal originating from the tip traveling over the hydrogel patches exceeded the lateral force signal over the substrate surface.

As with height images, the information contained in LFM images was condensed into lateral force signal distributions. The hydrogel patches and substrate regions of the sample were selected with the masks used in the height distribution analysis. The lateral force signal distributions for the sample shown in Figure 9a acquired at different normal loads F_n are shown in Figure 9b. As expected, with the increase in F_n, the S_L distributions shifted toward higher values, reflecting the familiar dependence of frictional force on normal load. Further analysis (data not shown) revealed that, for both the sample and the substrate, the mean frictional force signal $\langle S_L \rangle$ increased linearly with the load F_n, with an intercept very close to zero, in agreement with Amonton's law, and pointing to the absence of a major additional load, for example, due to tip−sample adhesion.[53] In further analysis, we have used the difference of slopes $\alpha_f = (d\langle S_L \rangle/dF_n)_{sample} - (d\langle S_L \rangle/dF_n)_{substrate}$. This, since the lateral force signal was not calibrated, could be referred to as the "uncalibrated differential friction coefficient of the sample versus the substrate". The plots of α_f as a function of temperature for samples **1** and **2** are shown in Figure 10.

In both cases, α_f initially increased with temperature, peaking between 45 and 50 °C and then sharply falling off. Such behavior can be viewed as an indication of an increase in the energy dissipation in the sample in the vicinity of the LCST transition.

Conclusions

Well-defined poly(DMAEMA-*stat*-BPMA) copolymers with different compositions were prepared via ATRP. The composition of the copolymer was controlled by adjusting the monomer feed ratio. When the resultant copolymers contained low BPMA content (≤5 mol %), a sharp phase transition in aqueous solution was observed with respect to the change in the environmental temperature. The copolymer containing 2.5 mol % of BPMA showed an LCST (35 °C) higher than the one containing 5 mol % of BPMA (33 °C). The photoactive BPMA units in the copolymers allow for the preparation of a patterned gel and immobilization on the Si substrate via UV treatment using a photomask technique. The thickness of the polymer pattern increased from 8 to 80 nm when the polymer solution concentration was increased from 2.5 to 20 g/L. The exposure time was found to be essential for the feature of patterning. The optimal exposure time was found to be 7.5 min under the applied experiment conditions.

CMAFM imaging of patterned hydrogel samples under water at different temperatures provided evidence of their thermal responsiveness, manifested as changes in the hydrogel patch heights. The use of different imaging forces made it possible to probe the hydrogel down to different depths, with the lowest forces probing just the uppermost layer, and higher forces probing the bulk of the hydrogel. The uppermost regions of characteristic nodules observed on the surface of the films collapsed at the temperature close to the LCST of free copolymer chains in solution, whereas the bulk of the film collapsed at the temperature almost 10 °C higher. The observed differences in the thermal response temperature at different depths of the hydrogel, most likely reflected the heterogeneity in cross-linking density (with the topmost layer being the least cross-linked). The thermal transition within the bulk of the film was also evident in lateral force imaging, where it was manifested as peaking of the apparent friction coefficient just above the transition temperature, indicating enhanced mechanical energy dissipation in the transition range. This observation points to the possibility of following the thermal transitions in stimulus-responsive hydrogels with proximal probe experiments monitoring mechanical energy dissipation. The observed enhanced ability of a thin LCST hydrogel films to dissipate mechanical energy near the transition could find use in the design of microfluidic devices and in the design of smart surfaces for tunable adhesive/frictional mechanical couplings.

Acknowledgment. The authors are grateful for the financial support provided by National Science Foundation (CTS-0304568), the Kosciuszko Foundation, and the members of the CRP Consortium at CMU.

LA061683K

(53) Gao, J.; Luedtke, W. D.; Gourdon, D.; Ruths, M.; Israelachvili, J. N.; Landman, U. *J. Phys. Chem. B* **2004**, *108*, 3410−3425.